Giant spin-torque generation by heavily oxidized Pt

Hongyu An, Yusuke Kanno, Akio Asami, and Kazuya Ando[*]
Department of Applied Physics and Physico-Informatics, Keio University, Yokohama 223-8522, Japan

(Received 9 May 2018; revised manuscript received 28 May 2018; published 2 July 2018)

We report a giant spin-torque generation originated from the ferromagnet/heavily oxidized Pt interface. The heavily oxidized Pt was fabricated by magnetron sputtering in a mixture of oxygen and argon gases with different oxygen flow rate Q from 50% to 100%. The dominant structure of the oxidized Pt is confirmed to be PtO_2 in this Q range. We show that even in this heavily oxidized range, robust dampinglike and fieldlike spin torques can still be generated from the $Ni_{81}Fe_{19}$/oxidized Pt interface. By increasing the oxidation level of the oxidized Pt, the generation efficiencies of both dampinglike and fieldlike torques increase drastically, and noticeably, a maximum generation efficiency of 0.92 for the dampinglike torque is obtained. Our study further demonstrates that the generation efficiency of the dampinglike torque has a much larger value than that of the fieldlike torque, which indicates a dominant generation of the dampinglike torque from the interface. Since no energy dissipation occurs in the bulk of the spin-torque generator, this study provides a piece of information for the development of the energy-efficient spin-orbit devices based on insulating metallic oxides.

DOI: 10.1103/PhysRevB.98.014401

I. INTRODUCTION

Spintronic devices are promising for application in future memory and logic technologies due to their high-speed response and low energy consumption [1–4]. In order to develop energy-efficient spintronic devices, the essential interest is to increase the generation efficiency of the spin-orbit torques from the charge current and to decrease the energy dissipation [5–14]. So far, topological insulators have been drawing attention as studies show their potential use as a spin-torque generator, which may significantly reduce the energy dissipation in the interior due to its bulk insulating property [15–21]. However, an ordinary insulator can also be expected to realize such purposes; nonzero spin torques can be generated in a heterostructure where a metallic magnet is sandwiched by two different insulators due to the broken inversion symmetry. In particular, metal oxides have been reported to have significant effects on the spin-torque generation. For instance, Emori *et al.* reported the sizable fieldlike torque generation from NiFe/Al_2O_3 and Cu/Al_2O_3 interfaces due to Rashba-Edelstein effects [22]. Demasius *et al.* reported a significant enhancement of the spin-torque generation by incorporating oxygen into tungsten and they interpreted that the enhancement was originated from the interface [13]. The spin-torque generation efficiency has been reported to be significantly enhanced by natural oxidation of Cu [23]. Gao *et al.* recently reported robust generation of the dampinglike torques in the $SiO_2/Ni_{81}Fe_{19}/CuO_x$ heterostructures arising from Berry curvature at the $Ni_{81}Fe_{19}/CuO_x$ interface [24]. Hibino *et al.* also reported an enhancement of the spin-torque generation by oxidizing the surface of the cobalt layer [25]. In our recent study, by incorporating oxygen into the widely used spintronic material, Pt, we observed a robust generation of spin-orbit torques in metallic magnet/oxidized Pt bilayer films [26]. The interface-induced robust spin-orbit torques can switch the magnetization of the magnet even if no charge current flows in the oxidized Pt, Pt(O). The Pt(O) film was fabricated in a mixture of oxygen and argon gases by rf magnetron sputtering, in which the relative oxygen flow rate Q was varied. In the previous study, we have systematically studied the spin-torque generation in a Q range from 0 to 35%. However, for a much higher Q range, a region where Pt is heavily oxidized, the spin-torque generation is still unclear.

In this work, we study the spin-torque generation by heavily oxidized Pt: Pt(O). Pt(O) was fabricated in a Q range from 50% to 100%. The dominant structure of Pt(O) in this range of Q is confirmed to be PtO_2. By conducting spin-orbit torque ferromagnetic resonance (ST-FMR) measurement, we show that compared with our previous study in the Q range from 0 to 35%, both dampinglike and fieldlike torque generation efficiencies have been enhanced by a maximum of two times. Furthermore, we found that the spin-orbit torque generation efficiency of Pt(O) is nearly an order of magnitude larger than that of Pt.

II. EXPERIMENTAL METHODS

The films were deposited on thermally oxidized Si substrates (SiO_2) by rf magnetron sputtering at room temperature. First, the Pt(O) layer was deposited on the SiO_2 substrate in a mixture of oxygen and argon gases with a total flow of 10 standard cubic centimeters per minute. For the deposition, oxygen and argon gases were introduced into the chamber, and the amount of oxygen gas in the mixture, Q, was varied from 50% to 100% to change the oxidation level of the Pt(O) films. Then, a 5-nm-thick $Ni_{81}Fe_{19}$ and a 4-nm-thick SiO_2 capping layer film were deposited by applying pure argon gas. The film thickness was controlled by the deposition time with a precalibrated deposition rate. For the fabrication of the devices used in the

[*]ando@appi.keio.ac.jp

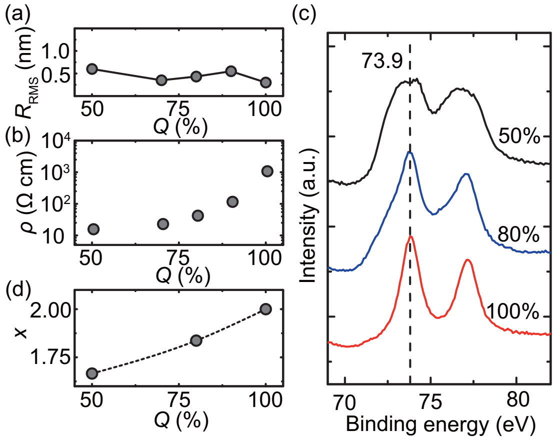

FIG. 1. (a) The surface roughness, (b) the resistivity, and (c) the XPS spectra of Pt(O) single-layer films with different Q. The binding energy of the Pt $4f$ peak at 73.9 eV in (b) indicates the existence of PtO_2 in Pt(O) films. (d) The oxygen stoichiometry $x = O/Pt$ with different Q in the Pt(O) films obtained from the XPS spectra. The dashed line is a guide for the eyes.

ST-FMR experiment, the substrates were patterned into a $16\ \mu m \times 40\ \mu m$ rectangular shape by photolithography before the deposition, and lift-off technique was used to remove the remaining part of the films after the deposition. Blanket Pt(O) single-layer films were used for the surface roughness measurement by atomic force microscopy (AFM) and the composition confirmation by x-ray photoelectron spectroscopy (XPS). All the measurements were conducted at room temperature.

III. RESULTS AND DISCUSSION

A deposition sequence of the SiO_2 capping layer/$Ni_{81}Fe_{19}$/Pt(O)/substrate was followed to avoid the oxidation of the $Ni_{81}Fe_{19}$ during the deposition. Since the Pt(O) layer was deposited in a range of high Q, the surface roughness of the Pt(O) layer may influence the spin-torque generation in the $Ni_{81}Fe_{19}$/Pt(O) bilayer films with different oxidation levels. Therefore, we first measured the surface roughness of Pt(O) single-layer films by AFM. As shown in Fig. 1(a), the surface root-mean-square roughness R_{RMS} in all the films with different Q are lower than 1 nm, indicating a smooth surface morphology of the Pt(O) films in the range of Q from 50% to 100%. Figure 1(b) shows the resistivity of the Pt(O) films, which increases with Q monotonically. The resistivity of Pt(O) films in this Q range (larger than $2.2 \times 10^7\ \mu\Omega$ cm) is much larger than that of $Ni_{81}Fe_{19}$ (106 $\mu\Omega$ cm). Therefore, the charge current flows in the Pt(O) layer can be neglected in the case of the $Ni_{81}Fe_{19}$/Pt(O) bilayer structure for the ST-FMR measurement. In order to investigate the composition of the Pt(O) films, the XPS measurement was conducted and the Pt $4f$ spectra were plotted in Fig. 1(c). A previous study on Pt(O) shows that binding energies of the Pt $4f$ peak for Pt^0, Pt^{2+}, and Pt^{4+} are around 71.3, 72.3, and 74.0 eV, respectively [27]. Thus, the peak of the initial Pt $4f$ spectrum at 73.9 eV in Fig. 1(c) indicates the formation of PtO_2 in the Pt(O) films. It is noticeable that by increasing Q from 50% to 100%, the full width half maximum of the spectra decreases. This is due to the existence of a minor portion of PtO in the Pt(O) film with $Q = 50\%$, which further reduces by increasing Q above 50% [27]. By fitting the XPS spectra, the oxygen stoichiometry $x = O/Pt$ with different Q was obtained as shown in Fig. 1(d).

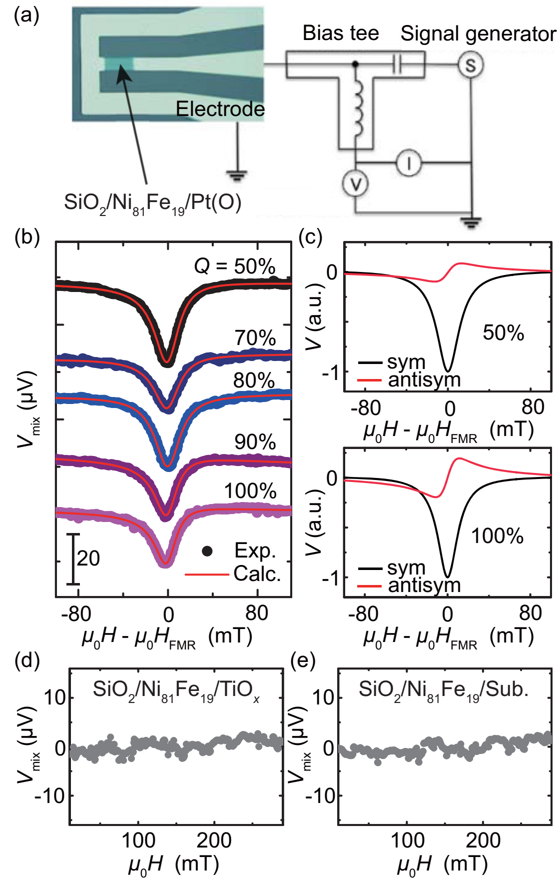

FIG. 2. (a) Schematic of the setup for ST-FMR measurement. (b) ST-FMR spectra for the $SiO_2/Ni_{81}Fe_{19}$/Pt(O) devices measured at 6 GHz by changing Q from 50% to 100%. The rf power of 24.7 dBm was applied for all the measurements. (c) The symmetric and antisymmetric components for $Q = 50\%$ and 100%. The symmetric component S was normalized and the antisymmetric component A divided by S was replotted for better comparison. (d) ST-FMR spectrum for the $SiO_2/Ni_{81}Fe_{19}/TiO_x$ device measured at 6 GHz. (e) ST-FMR spectrum for the $SiO_2/Ni_{81}Fe_{19}$/Sub. device measured at 6 GHz.

Figure 2(a) shows the schematic of the setup for the ST-FMR measurement. An rf charge current was applied along the longitudinal direction, and an in-plane external magnetic field **H** with an angle of 45° from the longitudinal direction of the device was applied. Since compared with $Ni_{81}Fe_{19}$, Pt(O) can be treated as a current-insulating layer, in the $Ni_{81}Fe_{19}$/Pt(O) bilayer structure, the rf current only generates dampinglike torque and fieldlike torque to drive magnetization precession in the $Ni_{81}Fe_{19}$ layer, and no Oersted field can be generated by the Pt(O) layer. The magnetization precession results in an oscillation of the resistance due to the anisotropic magnetoresistance in the $Ni_{81}Fe_{19}$ layer, which can be measured by using a bias tee.

The measured mixing dc voltage V_{mix} is expressed as [28–32]

$$V_{\mathrm{mix}} = S\frac{W^2}{(\mu_0 H - \mu_0 H_{\mathrm{FMR}})^2 + W^2} + A\frac{W(\mu_0 H - \mu_0 H_{\mathrm{FMR}})}{(\mu_0 H - \mu_0 H_{\mathrm{FMR}})^2 + W^2}, \quad (1)$$

where W and H_{FMR} are the spectral width and the FMR field, respectively. Here, S is the magnitude of the symmetric component of V_{mix} and A is the peak-to-dip value of the antisymmetric component of V_{mix}. In the ST-FMR signal, the symmetric component S is proportional to the dampinglike spin-orbit effective field H_{DL} [30,31]:

$$S = \frac{I_{\mathrm{rf}}\Delta R}{2\sqrt{2}}\mu_0 H_{\mathrm{DL}} A_{\mathrm{sym}}, \quad (2)$$

where

$$A_{\mathrm{sym}} = \frac{\mu_0 H_{\mathrm{FMR}} + \mu_0 M_{\mathrm{s}}}{W(2\mu_0 H_{\mathrm{FMR}} + \mu_0 M_{\mathrm{s}})}\sqrt{\frac{\mu_0 H_{\mathrm{FMR}}}{\mu_0 H_{\mathrm{FMR}} + \mu_0 M_{\mathrm{s}}}}. \quad (3)$$

Here, I_{rf} and ΔR are the rf current flowing in the bilayer and the resistance change of the bilayer due to the anisotropic magnetoresistance, respectively. M_{s} is the saturation magnetization of the $Ni_{81}Fe_{19}$ layer. Since in the $Ni_{81}Fe_{19}$/Pt(O) bilayer the Oersted field due to the current flow in the Pt(O) is negligible, the antisymmetric component A is proportional to the fieldlike spin-orbit effective field H_{FL} [30,31]:

$$A = \frac{I_{\mathrm{rf}}\Delta R}{2\sqrt{2}}\mu_0 H_{\mathrm{FL}} A_{\mathrm{asy}}, \quad (4)$$

where

$$A_{\mathrm{asy}} = \frac{\mu_0 H_{\mathrm{FMR}} + \mu_0 M_{\mathrm{s}}}{W(2\mu_0 H_{\mathrm{FMR}} + \mu_0 M_{\mathrm{s}})}. \quad (5)$$

Therefore, the relative magnitude of the fieldlike effective field H_{FL} to the dampinglike effective field H_{DL} can be directly obtained from the A/S ratio using

$$\frac{H_{\mathrm{FL}}}{H_{\mathrm{DL}}} = \frac{A}{S}\left(1 + \frac{\mu_0 M_{\mathrm{s}}}{\mu_0 H_{\mathrm{FMR}}}\right)^{-1/2}. \quad (6)$$

Figure 2(b) shows the ST-FMR spectra V_{mix} for the $SiO_2/Ni_{81}Fe_{19}$/Pt(O) devices with Q from 50% to 100% at 6 GHz. As can be seen, despite the absence of the charge current in the interior of the Pt(O) layer, ST-FMR signals can still be clearly observed in all the devices, which is consistent with our previous study [26]. We also fabricated SiO_2(4 nm)/$Ni_{81}Fe_{19}$ (5 nm)/TiO_x(8 nm) and SiO_2(4 nm)/$Ni_{81}Fe_{19}$(5 nm)/Sub. devices and conducted the ST-FMR experiments. As shown in Figs. 2(d) and 2(e), despite the magnetic resonance field around 106 mT for the $Ni_{81}Fe_{19}$ at 6 GHz, no signal can be observed. This result confirms that the large ST-FMR signal in Fig. 2(b) is originated from the $Ni_{81}Fe_{19}$/Pt(O) interface. In order to investigate the influence of Q on the spin-torque generation, we fitted the spectra with Eq. (1). Figures 2(c) and 2(d) exhibit A and S components separately in the case of $Q = 50\%$ and 100%. From this result, we obtained the relative magnitude of the fieldlike effective field H_{FL} to the dampinglike effective field H_{DL}, $|H_{\mathrm{FL}}/H_{\mathrm{DL}}| = 0.089$ and 0.21 for the $Ni_{81}Fe_{19}$/Pt(O) bilayer with $Q = 50\%$ and 100%, respectively. For a better comparison, $|H_{\mathrm{FL}}/H_{\mathrm{DL}}|$ is summarized in Fig. 3(a). Notably, $|H_{\mathrm{FL}}/H_{\mathrm{DL}}|$ increases by increasing Q.

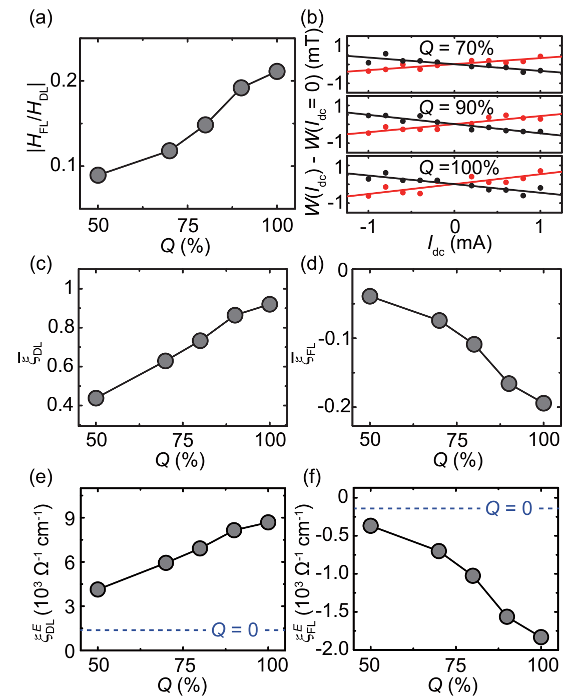

FIG. 3. (a) Q dependence of the ratio between antisymmetric component A and symmetric component S. (b) The change of the linewidth $W(I_{\mathrm{dc}})$ of the ST-FMR spectrum as a function of the applied dc current I_{dc} for different Q. The black and red solid circles represent the linewidth change measured by applying the negative and positive field, respectively. The black and red lines are the corresponding linear fits. (c) $\bar{\xi}_{\mathrm{DL}}$ and (d) $\bar{\xi}_{\mathrm{FL}}$ for different Q. (e) and (f) are the corresponding dampinglike and fieldlike torque generation efficiencies per unit applied electric field E.

Next, we evaluate the dampinglike and the fieldlike torque generation efficiencies. Since no current flows in the Pt(O) layer, the generally used dampinglike torque efficiency ξ_{DL} and the fieldlike torque efficiency ξ_{FL}, which are defined as the generation efficiency of the spin torques from the charge current density $j_{\mathrm{c}}^{\mathrm{Pt(O)}}$ flowing in the Pt(O) layer, cannot be calculated in the absence of $j_{\mathrm{c}}^{\mathrm{Pt(O)}}$. To evaluate the generation efficiency of the dampinglike and fieldlike torques, we conducted the ST-FMR experiment by applying a dc charge current I_{dc}. The dampinglike torque generated by the dc charge current I_{dc} effectively changes the magnetic damping α of the $Ni_{81}Fe_{19}$ layer or the FMR spectral width W, as shown in Fig. 3(b), which enables the determination of the conversion efficiency from I_{dc} to the dampinglike effective field H_{DL}. Since the charge current flows only in the $Ni_{81}Fe_{19}$ layer, the damping modulation allows one to determine the generation efficiency of the dampinglike torque from the charge current density $j_{\mathrm{c}}^{\mathrm{Py}}$ flowing in the $Ni_{81}Fe_{19}$ layer: $\bar{\xi}_{\mathrm{DL}} = \mu_0 M_{\mathrm{s}} d_{\mathrm{F}} H_{\mathrm{DL}}(2e/\hbar)/j_{\mathrm{c}}^{\mathrm{Py}}$, which is different from $\xi_{\mathrm{DL}} = \mu_0 M_{\mathrm{s}} d_{\mathrm{F}} H_{\mathrm{DL}}(2e/\hbar)/j_{\mathrm{c}}^{\mathrm{Pt(O)}}$. Here, the dependence of the change of the damping constant $\Delta\alpha$ on the applied dc charge current I_{dc} is expressed as [28]

$$\frac{\Delta\alpha}{I_{\mathrm{dc}}} = \frac{\hbar}{2e}\frac{\bar{\xi}_{\mathrm{DL}}}{\sqrt{2}M_{\mathrm{s}} w d_{\mathrm{F}}{}^2(\mu_0 H_{\mathrm{FMR}} + 0.5\mu_0 M_{\mathrm{s}})}, \quad (7)$$

where d_F and w are the thickness and width of the $Ni_{81}Fe_{19}$ layer. Using Eq. (7), we determined the dampinglike torque generation efficiency $\bar{\xi}_{DL}$ as shown in Fig. 3(c). Because of $\bar{\xi}_{FL}/\bar{\xi}_{DL} = H_{FL}/H_{DL}$, the fieldlike torque generation efficiency, $\bar{\xi}_{FL} = \mu_0 M_s d_F H_{FL}(2e/\hbar)/j_c^{Py}$, can also be determined as shown in Fig. 3(d).

Figures 3(c) and 3(d) show that by increasing Q from 50% to 100%, $\bar{\xi}_{DL}$ drastically increases from 0.44 to 0.92 and $\bar{\xi}_{FL}$ increases from −0.039 to −0.19. In order to verify whether the spin-torque generation efficiency is affected by the Pt(O) thickness, we further conducted the damping modulation experiment on a SiO_2(4 nm)/$Ni_{81}Fe_{19}$(5 nm)/Pt(O)(32 nm) device with $Q = 50\%$, where the Pt(O) thickness is two times larger compared with the current device. $\bar{\xi}_{DL}$ and $\bar{\xi}_{FL}$ were obtained as 0.46 and −0.044, respectively. The minor change of $\bar{\xi}_{DL}$ and $\bar{\xi}_{FL}$ confirms that the spin-torque generation is originated from the $Ni_{81}Fe_{19}$/Pt(O) interface and independent of the insulating Pt(O) thickness. It is noticeable that by increasing Q, although both $\bar{\xi}_{DL}$ and $\bar{\xi}_{FL}$ increase, the former always demonstrates a much larger value than the latter. This result is contrary to the prediction of the spin torques generated by the interface Rashba effect, which suggests a dominant generation of fieldlike torque [33,34]. In the study by Emori *et al.* [22], for the NiFe/Al_2O_3 and Cu/Al_2O_3 interfaces, only the fieldlike torque due to the Rashba-Edelstein effect was observed. In contrast to these systems, we observed the sizable dampinglike torque, which is several times larger than the fieldlike torque, in the $Ni_{81}Fe_{19}$/Pt(O) bilayer. Therefore, a new mechanism responsible for the dominant generation of the dampinglike torque from the $Ni_{81}Fe_{19}$/Pt(O) interface is required to explain our result.

Recent theoretical and experimental studies demonstrate that the generation of the intrinsic spin-orbit torques originated from the Berry curvature at interfaces can produce sizable dampinglike components [35,36]. Furthermore, Gao *et al.* reported the observation of the dampinglike torque arising from the Berry curvature in $Ni_{81}Fe_{19}/CuO_x$ bilayer films [24]. In their study, although both dampinglike and fieldlike torques are generated from the $Ni_{81}Fe_{19}/CuO_x$ interface, the former is an order of magnitude larger than the latter despite the absence of the current flowing in the CuO_x layer, which is consistent with our result.

The semi-insulating feature of the Pt(O) layer and the large dampinglike torque generation efficiency observed in the $Ni_{81}Fe_{19}$/Pt(O) bilayer provide evidence that the intrinsic Berry curvature mechanism due to the interface spin-orbit coupling is dominant in the spin-torque generation. The high electrical resistivity of the Pt(O) layer indicates that the applied charge current flows only in the $Ni_{81}Fe_{19}$ layer. In this condition, the dampinglike torque originating from the spin Hall effect in the Pt(O) layer through the spin-transfer mechanism can be neglected. Thus, only the spin-orbit coupling at the $Ni_{81}Fe_{19}$/Pt(O) interface can be the source of the observed spin-orbit torque. Although recent theoretical studies predict that a sizable dampinglike torque due to the interface spin-orbit coupling can be generated by spin-dependent scattering in a ferromagnetic-metal/heavy-metal bilayer, the dampinglike torque arising from this mechanism disappears in ferromagnetic-metal/insulator bilayers [37]. This indicates that the extrinsic mechanism of the spin-orbit torque generation does not result in the efficient generation of the dampinglike torque in the $Ni_{81}Fe_{19}$/Pt(O) bilayer. Therefore, the large dampinglike torque efficiency without using the bulk charge current observed in the $Ni_{81}Fe_{19}$/Pt(O) bilayer can only be explained by the intrinsic Berry curvature mechanism.

The spin-torque generation efficiency of the heavily oxidized Pt(O) is much larger than that of Pt, the most widely used heavy metal as a spin-torque source. By measuring the ST-FMR, we obtained the dampinglike and fieldlike torque generation efficiencies for a $Ni_{81}Fe_{19}$(6 nm)/Pt(8 nm) bilayer as $\xi_{DL} = 0.044$ and $\xi_{FL} = -0.0042$, where $\xi_{DL(FL)} = \mu_0 M_s d_F H_{DL(FL)}(2e/\hbar)/j_c^{Pt}$. These values are comparable to the spin-torque generation efficiencies reported previously [28,32]. Here, the spin-torque generation efficiencies $\xi_{DL(FL)}$ for the $Ni_{81}Fe_{19}$/Pt bilayer cannot be compared directly with $\bar{\xi}_{DL(FL)}$ for the $Ni_{81}Fe_{19}$/Pt(O) bilayer. To compare the generation of the spin-orbit torques between the $Ni_{81}Fe_{19}$/Pt and $Ni_{81}Fe_{19}$/Pt(O) bilayers, we define the spin-torque generation efficiency per unit applied electric field E [38]:

$$\xi^E_{DL(FL)} = \frac{2e}{\hbar}\mu_0 M_s d_F \frac{H_{DL(FL)}}{E}. \tag{8}$$

Here, for the $Ni_{81}Fe_{19}$/Pt bilayer, $\xi^E_{DL(FL)}$ can be obtained using $\xi^E_{DL(FL)} = \xi_{DL(FL)}/\rho_{Pt}$: $\xi^E_{DL} = 1.4 \times 10^3\ \Omega^{-1}\,cm^{-1}$ and $\xi^E_{FL} = -0.13 \times 10^3\ \Omega^{-1}\,cm^{-1}$, where ρ_{Pt} is the resistivity of the Pt layer (32 $\mu\Omega$ cm). For the $Ni_{81}Fe_{19}$/Pt(O) bilayer, using $\xi^E_{DL(FL)} = \bar{\xi}_{DL(FL)}/\rho_{Py}$, we obtained Q dependence of $\xi^E_{DL(FL)}$ as shown in Figs. 3(e) and 3(f), where ρ_{Py} is the resistivity of the $Ni_{81}Fe_{19}$ layer. As shown in Figs. 3(e) and 3(f), for the $Ni_{81}Fe_{19}$/Pt(O) bilayer with $Q = 100\%$, we obtained $\xi^E_{DL} = 8.7 \times 10^3\ \Omega^{-1}\,cm^{-1}$ and $\xi^E_{FL} = -1.8 \times 10^3\ \Omega^{-1}\,cm^{-1}$, nearly an order of magnitude larger than $\xi^E_{DL(FL)}$ of Pt. In spintronics, Pt has been known as one of the most efficient spin-torque sources. This result demonstrates that the generation efficiency of the spin-orbit torque can further be enhanced by the oxidation, promising a route for exploring efficient spin-torque generators through the oxidation of heavy metals. We have also compared our result with the study by Gao *et al.* [24]. The spin-torque generation efficiency of the $Ni_{81}Fe_{19}$/Pt(O) bilayer ($\xi^E_{DL} = 8.7 \times 10^3\ \Omega^{-1}\,cm^{-1}$) is significantly larger than that of the $Ni_{81}Fe_{19}/CuO_x$ bilayer ($\xi^E_{DL} = 20\ \Omega^{-1}\,cm^{-1}$), which makes the $Ni_{81}Fe_{19}$/Pt(O) bilayer an appealing system for the application of spin orbitronics.

IV. CONCLUSIONS

In summary, we have studied the spin-torque generation by heavily oxidized Pt: Pt(O). The Pt(O) films were fabricated with different oxygen flow rate Q in a mixture of oxygen and argon gases from 50% to 100% by magnetron sputtering. The dominant structure of Pt(O) in this Q range is confirmed to be PtO_2. By attaching a ferromagnetic layer $Ni_{81}Fe_{19}$ to the Pt(O), we show that without charge current flowing in the Pt(O) layer, robust dampinglike and fieldlike spin torques can still be generated from the interface of $Ni_{81}Fe_{19}$/Pt(O). Further study shows that the generation efficiencies of both dampinglike and fieldlike torques increase by increasing Q. Compared with our previous study in the Q range from 0 to 35%, both dampinglike and fieldlike torque generation efficiencies have been enhanced by a maximum of two times. In particular, the dampinglike torque generation efficiency reaches 0.92 when Q is 100%, which is much larger than the generally used heavy metals. This can drastically reduce the current density requested for the current-induced magnetization switching. Since no energy dissipation occurs in the bulk of the spin-torque generator, our study promotes the development of the energy-efficient spin-orbit devices based on insulating metallic oxides.

ACKNOWLEDGMENTS

This work was supported by JSPS KAKENHI Grants No. 26220604 and No. 26103004, the Asahi Glass Foundation, JSPS Core-to-Core Program, and Spintronics Research Network of Japan (Spin-RNJ). H.A. is JSPS International Research Fellow and acknowledges the support from the JSPS Fellowship (No. P17066 and No. 17F17066).

[1] J. Sinova, S. O. Valenzuela, J. Wunderlich, C. H. Back, and T. Jungwirth, Rev. Mod. Phys. **87**, 1213 (2015).
[2] T. Jungwirth, J. Wunderlich, and K. Olejnik, Nat. Mater. **11**, 382 (2012).
[3] A. Manchon, H. C. Koo, J. Nitta, S. M. Frolov, and R. A. Duine, Nat. Mater. **14**, 871 (2015).
[4] A. Soumyanarayanan, N. Reyren, A. Fert, and C. Panagopoulos, Nature (London) **539**, 509 (2016).
[5] I. M. Miron, K. Garello, G. Gaudin, P.-J. Zermatten, M. V. Costache, S. Auffret, S. Bandiera, B. Rodmacq, A. Schuhl, and P. Gambardella, Nature (London) **476**, 189 (2011).
[6] I. M. Miron, G. Gaudin, S. Auffret, B. Rodmacq, A. Schuhl, S. Pizzini, J. Vogel, and P. Gambardella, Nat. Mater. **9**, 230 (2010).
[7] L. Liu, C.-F. Pai, Y. Li, H. Tseng, D. Ralph, and R. Buhrman, Science **336**, 555 (2012).
[8] J. Kim, J. Sinha, M. Hayashi, M. Yamanouchi, S. Fukami, T. Suzuki, S. Mitani, and H. Ohno, Nat. Mater. **12**, 240 (2013).
[9] G. Yu, P. Upadhyaya, Y. Fan, J. G. Alzate, W. Jiang, K. L. Wong, S. Takei, S. A. Bender, L.-T. Chang, Y. Jiang, M. Lang, J. Tang, Y. Wang, Y. Tserkovnyak, P. K. Amiri, and K. L. Wang, Nat. Nanotechnol. **9**, 548 (2014).
[10] X. Wang, C. O. Pauyac, and A. Manchon, Phys. Rev. B **89**, 054405 (2014).
[11] K. Garello, I. M. Miron, C. O. Avci, F. Freimuth, Y. Mokrousov, S. Blügel, S. Auffret, O. Boulle, G. Gaudin, and P. Gambardella, Nat. Nanotechnol. **8**, 587 (2013).
[12] X. Fan, J. Wu, Y. Chen, M. J. Jerry, H. Zhang, and J. Q. Xiao, Nat. Commun. **4**, 1799 (2013).
[13] K.-U. Demasius, T. Phung, W. Zhang, B. P. Hughes, S.-H. Yang, A. Kellock, W. Han, A. Pushp, and S. S. Parkin, Nat. Commun. **7**, 10644 (2016).
[14] M. Akyol, J. G. Alzate, G. Yu, P. Upadhyaya, K. L. Wong, A. Ekicibil, P. K. Amiri, and K. L. Wang, Appl. Phys. Lett. **106**, 032406 (2015).
[15] A. Mellnik, J. Lee, A. Richardella, J. Grab, P. Mintun, M. Fischer, A. Vaezi, A. Manchon, E.-A. Kim, N. Samarth, and D. C. Ralph, Nature (London) **511**, 449 (2014).
[16] Y. Fan, P. Upadhyaya, X. Kou, M. Lang, S. Takei, Z. Wang, J. Tang, L. He, L.-T. Chang, M. Montazeri, G. Yu, W. Jiang, T. Nie, R. N. Schwartz, Y. Tserkovnyak, and K. L. Wang, Nat. Mater. **13**, 699 (2014).
[17] Y. Fan, X. Kou, P. Upadhyaya, Q. Shao, L. Pan, M. Lang, X. Che, J. Tang, M. Montazeri, K. Murata, L.-T. Chang, M. Akyol, G. Yu, T. Nie, K. L. Wong, J. Liu, Y. Wang, Y. Tserkovnyak, and K. L. Wang, Nat. Nanotechnol. **11**, 352 (2016).
[18] K. Kondou, R. Yoshimi, A. Tsukazaki, Y. Fukuma, J. Matsuno, K. Takahashi, M. Kawasaki, Y. Tokura, and Y. Otani, Nat. Phys. **12**, 1027 (2016).
[19] J. Han, A. Richardella, S. A. Siddiqui, J. Finley, N. Samarth, and L. Liu, Phys. Rev. Lett. **119**, 077702 (2017).
[20] Y. Wang, D. Zhu, Y. Wu, Y. Yang, J. Yu, R. Ramaswamy, R. Mishra, S. Shi, M. Elyasi, K.-L. Teo, Y. Wu, and H. Yang, Nat. Commun. **8**, 1364 (2017).
[21] S. Shi, A. Wang, Y. Wang, R. Ramaswamy, L. Shen, J. Moon, D. Zhu, J. Yu, S. Oh, Y. Feng, and H. Yang, Phys. Rev. B **97**, 041115 (2018).
[22] S. Emori, T. Nan, A. M. Belkessam, X. Wang, A. D. Matyushov, C. J. Babroski, Y. Gao, H. Lin, and N. X. Sun, Phys. Rev. B **93**, 180402 (2016).
[23] H. An, Y. Kageyama, Y. Kanno, N. Enishi, and K. Ando, Nat. Commun. **7**, 13069 (2016).
[24] T. Gao, A. Qaiumzadeh, H. An, A. Musha, Y. Kageyama, J. Shi, and K. Ando, arXiv:1802.01285.
[25] Y. Hibino, T. Hirai, K. Hasegawa, T. Koyama, and D. Chiba, Appl. Phys. Lett. **111**, 132404 (2017).
[26] H. An, T. Ohno, Y. Kanno, Y. Kageyama, Y. Monnai, H. Maki, J. Shi, and K. Ando, Sci. Adv. **4**, aar2250 (2018).
[27] D. Svintsitskiy, L. Kibis, A. Stadnichenko, S. Koscheev, V. Zaikovskii, and A. Boronin, Chem. Phys. Chem. **16**, 3318 (2015).
[28] L. Liu, T. Moriyama, D. C. Ralph, and R. A. Buhrman, Phys. Rev. Lett. **106**, 036601 (2011).
[29] W. Zhang, W. Han, X. Jiang, S.-H. Yang, and S. S. Parkin, Nat. Phys. **11**, 496 (2015).
[30] V. Tshitoyan, C. Ciccarelli, A. P. Mihai, M. Ali, A. C. Irvine, T. A. Moore, T. Jungwirth, and A. J. Ferguson, Phys. Rev. B **92**, 214406 (2015).
[31] D. Fang, H. Kurebayashi, J. Wunderlich, K. Výborný, L. Zârbo, R. Campion, A. Casiraghi, B. Gallagher, T. Jungwirth, and A. Ferguson, Nat. Nanotechnol. **6**, 413 (2011).
[32] C.-F. Pai, Y. Ou, L. H. Vilela-Leão, D. C. Ralph, and R. A. Buhrman, Phys. Rev. B **92**, 064426 (2015).
[33] P. M. Haney, H.-W. Lee, K.-J. Lee, A. Manchon, and M. D. Stiles, Phys. Rev. B **87**, 174411 (2013).
[34] D. A. Pesin and A. H. MacDonald, Phys. Rev. B **86**, 014416 (2012).
[35] H. Kurebayashi, J. Sinova, D. Fang, A. C. Irvine, T. D. Skinner, J. Wunderlich, V. Novák, R. P. Campion, B. L. Gallagher, E. K. Vehstedt, L. P. Zârbo, K. Výborný, A. J. Ferguson, and T. Jungwirth, Nat. Nanotechnol. **9**, 211 (2014).
[36] H. Li, H. Gao, L. P. Zârbo, K. Výborný, X. Wang, I. Garate, F. Doğan, A. Čejchan, J. Sinova, T. Jungwirth, and A. Manchon, Phys. Rev. B **91**, 134402 (2015).
[37] K.-W. Kim, K.-J. Lee, J. Sinova, H.-W. Lee, and M. D. Stiles, Phys. Rev. B **96**, 104438 (2017).
[38] M.-H. Nguyen, D. C. Ralph, and R. A. Buhrman, Phys. Rev. Lett. **116**, 126601 (2016).